High-Precision XY Stage Motion Control of Industrial Microscope

Idris Li Hong Lim, *Member*, and Dazhi Yang

Post Conference Paper

***Abstract*—This paper presents an economic way to implement a high precision (μm level) XY stage motion control for the industrial microscope using DC motors. Other than the prevailing design of using stepper motors where the stage is always locked under the motorized mode, the proposed design allows users to manually move the stage by introducing the friction engagement in between. The nonlinearity from the friction is then fully compensated by the sliding mode control (SMC) so that the stage can strictly follow the predefined motion profile. Possible chattering suppression methods are discussed and the accuracy loss is analyzed using LuGre friction model. Fine-tuning algorithm is then proposed to limit the position error within ± 2 μm. Comparing to the other μm-level industrial microscopes using stepper motors, the proposed solution achieves comparable performance with much lower costs.**

***Index Terms*—SMC, DC motor, microscope.**

I. Introduction

WITH the rapid progress of optics and zoom design, the magnification of a modern industrial microscope can be up to 2350×, which greatly expands its application in the industry of semiconductor, automotive, biomedical, etc. The big magnification requires the high precision (e.g., μm-level) for XY stage motion, and the conventional manual stage becomes less competent in such a case. Correspondingly, the motorized stage is a better choice, where stepper motors are broadly used due to their precise structure and simplicity in control (usually open-loop). Recent progress in motorized stage design can even achieve nano precision and large-range motion by using compliant mechanisms [1]–[3]. However, the microscope is not always working under big magnifications. For low and mid magnifications, manual stage movement is still preferred due to its convenience and fast response, which means the motor must allow manual rotation during the operation. Unfortunately, this is not applicable for stepper motors as well as other actuation technology like linear or piezo motors.

In order to allow manual movement for a motorized stage, the DC motor seems to be the only choice. Recent patent [4] proposed a stage design using DC motors and the friction as the driving force. The engagement of friction brings a big challenge to the motion control. As shown in Fig. 1(a), friction can be modeled as a nonlinear function of relative velocity, which is composed of Stribeck (between static and Coulomb), Coulomb, and viscous components [5]. In reality, Stribeck friction can even vary in the phase of acceleration and deceleration, as shown in Fig. 1(b). Such a high nonlinearity can cause system damping (see more details in Fig. 9). Therefore, linear controller like PID is inapplicable. Since the friction is either unknown or unmeasurable, feed forward compensation is inapplicable as well. If the uneven contact surface along the stage rod is considered, Coulomb friction is not constant anymore, which makes control more difficult.

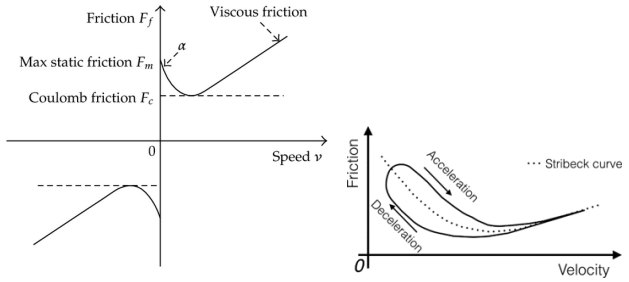

(a) model (b) real

Fig. 1. Friction modeling

A natural question is whether the solution in [4] can achieve the μm-level precision of the stage motion. If possible, what's the lowest cost? The ideal case is that all the necessary hardware components are kept unchanged to maintain the low cost, and only control algorithm in firmware is changed to achieve μm-level precision. That's the motivation of the paper and our way to implement "high-precision-low-cost" motion control for XY stage.

If the friction is regarded as some external disturbance, the motion control of the DC motor is equivalent to the disturbance rejection, and sliding mode control (SMC) should be applicable in that case. SMC in nature is a nonlinear control [6], which constraints the system motion in a manifold (sliding surface) to simplify the system (order reduction). It is also independent of matched disturbance, so detailed information about friction is not required, except for its upper bound only. The control law is simple enough to be easily implemented (no integral calculation like PID) and very robust,

Idris Li Hong Lim is with the Department of Electronic Systems, University of Glasgow, Glasgow G12 8QQ, UK (corresponding author. e-mail: LiHonIdris.Lim@glasgow.ac.uk).

Dazhi Yang is with Singapore Institute of Manufacturing Technology, 71 Nanyang Drive, Singapore 638705.

so no extra requirements or costs are needed for the hardware manufacturing.

The main obstacle of applying SMC in practice is the so-called chattering [7], which is caused by the discontinuous function $\mathrm{sgn}(\sigma)$ in the control $u(t)$, where σ is the sliding surface. As $\sigma \to 0$, $\mathrm{sgn}(\sigma)$ will be fast switching between ± 1, which results in unacceptable noise as well as damages to the device. Increasing the sampling rate helps to alleviate the chattering, but it cannot eliminate the root cause. Boundary layer design [8] is a commonly used method for chattering suppression, where a continuous saturation function $\mathrm{sat}(\cdot)$ replaces the discontinuous sign function $\mathrm{sgn}(\cdot)$ in a region called the boundary layer around the sliding surface. However, using $\mathrm{sat}(\cdot)$ instead of $\mathrm{sgn}(\cdot)$ breaks the asymptotic stability of SMC (i.e., $\sigma \to 0$ as $t \to \infty$) so that accuracy loss is inevitable. Recent progress in chattering suppression is well summarized in [9]–[11], where existing methods can be divided into two categories. One is to introduce an integrator in SMC so that discontinuous functions after integral become continuous [12]–[14]. The other is to increase the order of SMC [15]–[17], based on which super twisting algorithm [18] is proposed and combined with adaptive change of control gain. However, both methods increase the complexity in control and difficulty in implementation. Extra cost for faster MCU and more RAM is also inevitable.

A better way is to use SMC with boundary layer as the coarse tuning for the motion control, which will drive the stage to some neighbourhood of target position. Then, some fine tuning method can be used to narrow the position error within the μm-level tolerance. The preliminary work was reported in IECON 2017 [19], and this paper includes the supplements for the fine-tuning analysis, simulation, precision comparison with PID and stepper motors.

The whole paper is organized as follows. Section II presents the hardware components of a commercially available XY stage, which serves as our bench mark. Standard SMC design with boundary layers is given in Section III, where fine tuning method is proposed and analyzed with LuGre friction model. Validation is done in Section IV by comparing the stage performance (both precision and speed) with its original PID control as well as the competitor's product. Conclusion is finally drawn in Section V.

II. Hardware Description

The proposed research is based on Leica DVM6, which is a good benchmark for our study since Leica is a leading brand and manual movement is allowed in their motorized XY stage. The experiment setup is shown in Fig. 2, where all the motion control is done by XYZ main PCB. MCU is from Freescale MC56F8335, which is 16-bit, 60 MHz maximum core frequency with 64KB program flash. It was lauched in 2007, cheap enough but less powerful now. Through CodeWarrior USB TAP, new firmware with the proposed control can be flashed back to MCU. Real-time data of the stage performance is then displayed in FreeMaster through UART debug port. Target position commands are set through CAN bus.

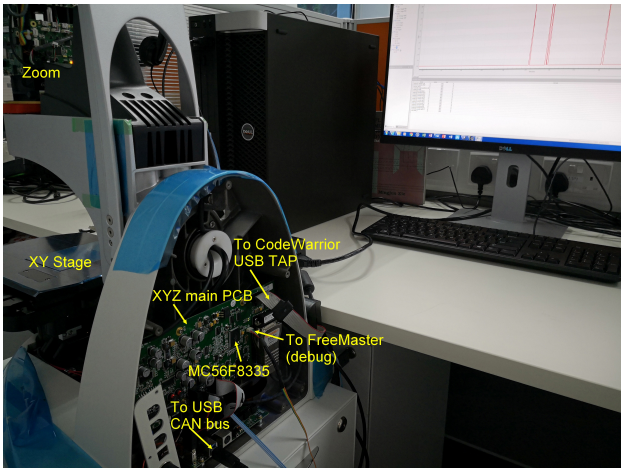

Fig. 2. Experiment setup

By tearing down the XY stage, the friction engagement between motor shafts and moving tracks can be simply diagrammed in Fig. 3(a), where DC motor is mounted on a bracket attached to a spring to keep the motor in position during motor operation. Roller bearings and springs are used to maintain a constant force exerted on the motor shaft against the parallel rod. Since DC motors are fixed to the XY stages, motor shaft moving along the rod (track) will pull the stage to move as well. The detailed schematic for the controlled XY stage is shown in Fig. 3(b), where each stage has two parallel rods on which bearings provide guidance and low friction as the driving force.

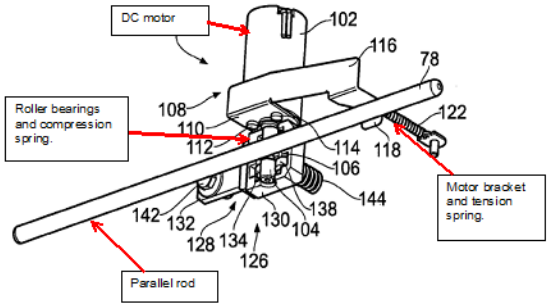

(a) friction engagement

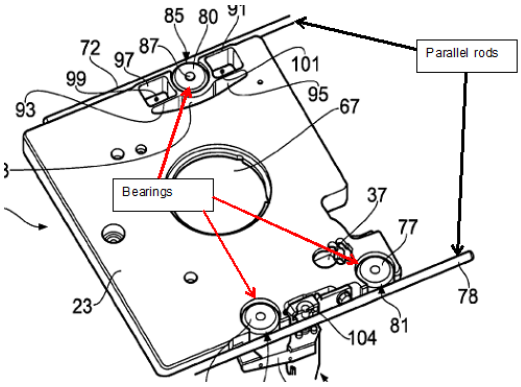

(b) stage schematic

Fig. 3. Diagram of XY stage [20]

In the case of the electronic components, optical scale/readhead from Renishaw gives the position encoder with the resolution of 0.2 μm, as shown in Fig. 4, where only X stage is demonstrated. An interpolator is used to digitalize the analog signal from the readhead. PCBA attached to the stage center is in charge of all the communication among encoder, motor and MCU. With the constraints of space and weight, coreless DC motor from Namiki is used. The hardware architecture of the stage positioning system is shown in Fig. 5.

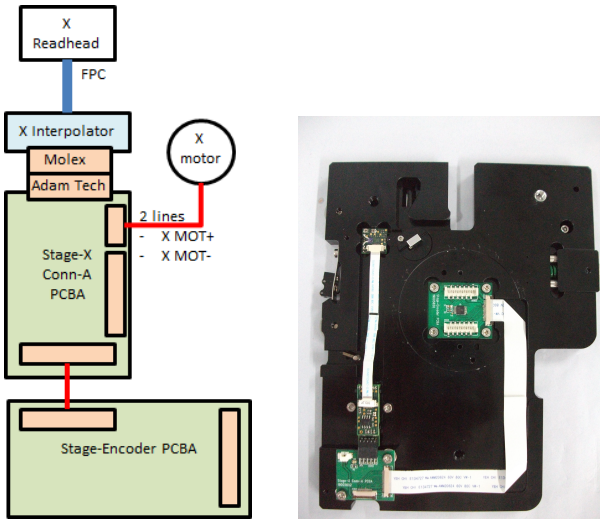

(a) Diagram (b) Real connection

Fig. 4. Optical encoder for position

The DVM6 with the original firmware has been extensively tested on the precision and speed, and the result can be found in Section IV. There exists about 1% cases that the target position cannot be met within the error tolerance of ± 2 μm. Speed profile of motion control is not strictly followed either as one can feel the obvious jitter during the stage movement. As mentioned in Introduction, the objective of this paper is to keep all the hardware unchanged, but to improve the stage performance by changing the firmware only (using SMC-based motion control).

III. Stage Motion Control with SMC

The system diagram of the motion control in DVM6 is shown in Fig. 6, where V is input voltage to DC motor; E is back electro-motive force (EMF); R and L are armature resistance and inductance, respectively; K_e is back EMF constant; K_t is torque constant; T and T_d are torque from motor and friction, respectively; J is rotor inertia; b is viscous friction constant; ω is angular velocity; θ is rotation angle; and r is the radius from rotor axis to the contact point on tracks. The real values of all parameters are shown in TABLE I.

A. Standard SMC Design

To simplify our design, let $b \approx 0$ as coreless DC motor is used here. Since the electrical time constant $\tau_e = L/R = 14.5$ μs, which is much less than the shortest sampling time of MCU (102 μs), dynamics in armature can be ignored, i.e., $1/(Ls+R) \approx 1/R$. In combination of the controller, Fig. 6(a) can be further simplified as Fig. 6(b), where r is put into the inner loop, y and y_r are the current and target position of the stage, respectively, and $e = y_r - y$ is the position error.

TABLE I
System Variables

Symbol	Value	Unit	Symbol	Value	Unit
L	0.16	mH	R	11	Ω
K_t	12.7	mNm/A	K_e	1.3	mV/rpm
J	1.1	gcm^2	r	1.542	mm

Let $x_1 = y$ and $x_2 = \dot{x}_1 = \dot{y}$, it derives from Fig. 6 that

$$\begin{aligned}\dot{x}_1 &= x_2,\\ \dot{x}_2 &= \left[\left(u - \frac{K_e}{r}x_2\right)\frac{K_t}{R} - T_d\right]\frac{r}{J}.\end{aligned}$$

Let $e_1 = e = y_r - y$ and $e_2 = \dot{e}_1$, then $x_1 = y = y_r - e_1$ and $x_2 = \dot{x}_1 = \dot{y}_r - e_2$. Replacing state variables x_1 and x_2 with e_1 and e_2 gives

$$\dot{e}_1 = e_2, \tag{1}$$

$$\dot{e}_2 = \ddot{y}_r + \frac{K_eK_t}{JR}\dot{y}_r - \frac{K_eK_t}{JR}e_2 - \frac{rK_t}{JR}u + \frac{r}{J}T_d. \tag{2}$$

Define the sliding surface $\sigma = p_1e_1 + p_2e_2$ with $p_{1,2} > 0$, it follows from (1) and (2) that

$$\begin{aligned}\dot{\sigma} = p_2&\left(\ddot{y}_r + \frac{K_eK_t}{JR}\dot{y}_r\right) + \left(p_1 - p_2\frac{K_eK_t}{JR}\right)e_2\\ &- p_2\frac{rK_t}{JR}u + p_2\frac{r}{J}T_d.\end{aligned} \tag{3}$$

If Friction is bounded, i.e., $0 < |T_d| \le T_m$, the SMC is given by

$$\begin{aligned}u = \frac{JR}{rK_t}&\left[\left(\ddot{y}_r + \frac{K_eK_t}{JR}\dot{y}_r\right)\right.\\ &\left. + \left(\frac{p_1}{p_2} - \frac{K_eK_t}{JR}\right)e_2 + \frac{\mu}{p_2}\mathrm{sgn}(\sigma)\right],\end{aligned} \tag{4}$$

where $\mu > T_mp_2r/J$. Substituting (4) into (3) yields

$$\dot{\sigma} = -\left[\mu\mathrm{sgn}(\sigma) - p_2\frac{r}{J}T_d\right]. \tag{5}$$

The proof of $e_{1,2} \to 0$ as $t \to \infty$ in (1) and (2) with SMC by (4) is standard. Choose Lyapunov function $V = \sigma^2/2 \ge 0$, it follows from (5) that

$$\begin{aligned}\dot{V} = \sigma\dot{\sigma} &= -\left(\mu|\sigma| - p_2\frac{r}{J}T_d\sigma\right)\\ &< -\left(p_2\frac{r}{J}T_m|\sigma| - p_2\frac{r}{J}T_d\sigma\right)\\ &\le -p_2\frac{r}{J}\left(|T_d||\sigma| - T_d\sigma\right) \le 0.\end{aligned}$$

B. Chattering Suppression

Chattering caused by SMC in (4) comes from the following factors.

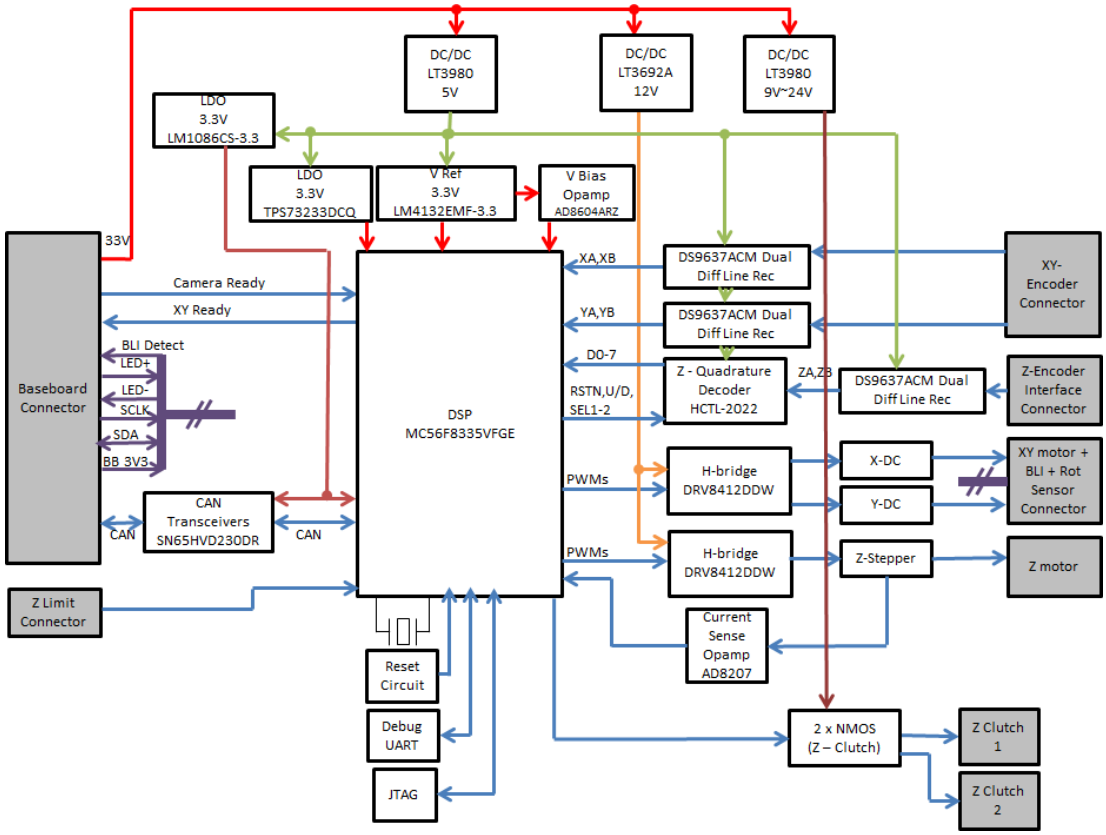

Fig. 5. Hardware architecture of stage motion control

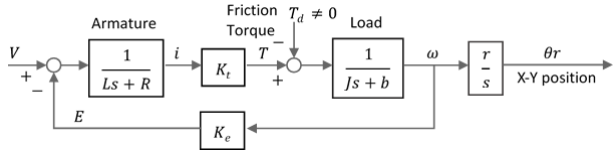

(a) DC motor system for DVM6

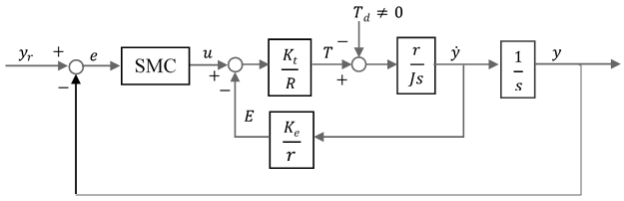

(b) Simplified motion control system with SMC

Fig. 6. Diagram of motion control systems

1) Noise in e_2: Only position sensor is available for XY stage of microscope, i.e., $e_1(t)$ is directly measured. To get $e_2(t)$, differentiation $[e_1(t) - e_1(t - T_s)]/T_s$ has to be done, which also magnifies the measurement error in e_1 especially for fast sampling system. Let

$$\frac{p_1}{p_2} - \frac{K_e K_t}{JR} = 0,$$

then (4) becomes

$$u = \frac{JR}{rK_t}\left[\left(\ddot{y}_r + \frac{K_e K_t}{JR}\dot{y}_r\right) + \frac{\mu}{p_2}\mathrm{sgn}(\sigma)\right],$$

which does not contain any e_2 term.

2) Over-estimation of μ: μ is dependent of T_m, which can be big enough as long as the hardware allows. However, a high T_m is unnecessary for most of our working conditions. Note that T_d mainly increases with motor speed, a more realistic way to lower μ is to limit motor speed by following a predefined profile. This is also the requirement of motion control. Fig. 7 shows the commonly used speed profile for motion control. If $e(0) \leq \int_0^{t_0} v\mathrm{d}t$, the speed profile is triangle. Otherwise, the speed profile is trapezoid.

According to the friction model (12) in Appendix,

$$\sigma_0 z = g(v)\mathrm{sgn}(v) - \frac{g(v)}{|v|}\dot{z}. \tag{6}$$

Substitue (6) into (13), the friction

$$F = g(v)\mathrm{sgn}(v) + \sigma_2 v + \left(\sigma_1 - \frac{g(v)}{|v|}\right)\dot{z}.$$

Since T_m corresponds to the constant v_m (when motor speed follows the trapezoid profile), $\dot{z} \approx 0$, then $F = g(v)\mathrm{sgn}(v) + \sigma_2 v$ and

$$\mu = T_m p_2 r/J \leq (|g(v_m)| + \sigma_2|v|)p_2 r^2/J.$$

3) Discontinuity of sgn Function: Boundary layer method is used to replace the discontinuous $sgn(\cdot)$ function with the continuous saturator function $sat(\cdot)$, as shown in Fig. 8(a). d is a tuning parameter to get the balance between the accuracy and performance requirements.

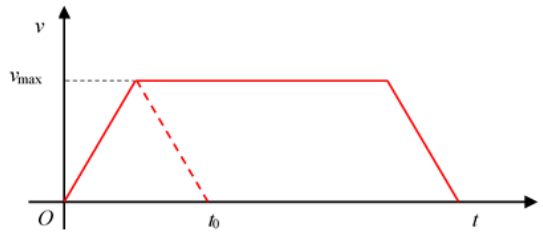

Fig. 7. Motor speed profile

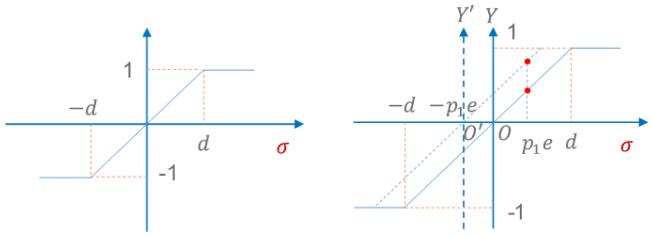

(a) sat(·) (b) fine-tuning

Fig. 8. Boundary layer method and fine-tuning

C. Fine-tuning Method

SMC with the boundary layers drives the stage into some neighbourhood of the target position with a radius less than d. After that, the proposed fine-tuning method further narrows the neighborhood radius within 2 μm. Friction plays an important role in this phase. Impulse response in Fig. 9 shows how the friction impacts on system dynamics, where the dotted blue line represents the real response for $T_d \neq 0$. Motor input

$$u(t) = \begin{cases} 12\text{ V}, & 0 < t < T_s; \\ 0\text{ V}, & \text{otherwise}, \end{cases}$$

where 12 V is the maximum input voltage of DC motor, and $T_s = 102$ μs is the fastest sampling time of MCU. If $T_d = 0$, the open-loop transfer function from u to y is

$$G(s) = \frac{Y(s)}{U(s)} = \frac{1}{s(\tau s + 1)},$$

where $\tau = JR/(rK_t)$ is the time constant. Its impulse response in time domain for $u(t) = K\delta(t)$ should be

$$y(t) = K(1 - \mathrm{e}^{-t/\tau}), \tag{7}$$

which is shown by the red line. It is clear to see that friction affects both steady and transient states of the system. Steady state value drops 96% from 150 μm to 6 μm. (7) has no damping at all, but friction causes damping up to 12 μm, which is much larger than the precision requirement of ± 2 μm.

As aforementioned, chattering suppression using boundary layer method suffers from the accuracy loss, i.e., $0 < |e| < d$. Suppose at $t = t_1$, the stage stops moving and enters the steady state, i.e., $e_1(t_1) = e(t_1)$, $e_2(t_1) = \dot{e}_1(t_1) = 0$ and $\dot{e}_2(t_1) = 0$. $\sigma(t_1) = p_1 e_1(t_1) + p_2 e_2(t_1) = p_1 e(t_1)$, and (4) becomes

$$u(t_1) = \frac{JR\mu}{rK_t p_2}\mathrm{sat}(p_1 e(t_1), d) = \frac{JR\mu p_1}{rK_t p_2} e(t_1), \tag{8}$$

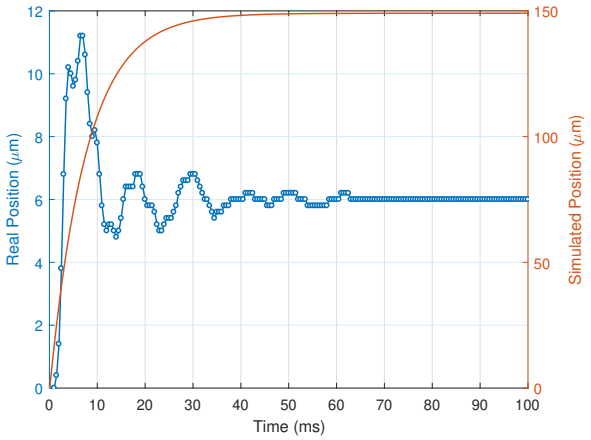

Fig. 9. System impulse response in case of friction

since $\ddot{y}_r(t_1) = \dot{y}_r(t_1) = 0$. Substitute (8) into (2),

$$\frac{r}{J} T_d(t_1) = \mu \frac{p_1}{p_2} e(t_1). \tag{9}$$

At $t = t_1^+$, if $\Delta u = u(t_1)$ is injected into $u(t)$, i.e., $u^*(t) = u(t) + u(t_1)$ for $t > t_1$, by LuGre model in Appendix from (12) and (13), $v(t_1^+) = 0$ and $\dot{z}(t_1^+) = 0$, so $F(t_1^+) = F(t_1) = \sigma_0 z(t_1)$ has no change. So does T_d as $T_d = F \times r$. However by (2),

$$\begin{aligned} \dot{e}_2(t_1^+) &= \frac{r}{J} T_d(t_1^+) - \frac{rK_t}{JR}\left[u(t_1^+) + u(t_1)\right] \\ &= \frac{r}{J} T_d(t_1^+) - \mu \frac{p_1}{p_2} e(t_1) - \frac{rK_t}{JR} u(t_1^+) \\ &= -\frac{rK_t}{JR} u(t_1^+) \neq 0, \end{aligned}$$

which means the stage starts to move. Suppose at $t = t_2$, the stage stops moving and enters the steady state again, i.e., $e_1(t_2) = e(t_2)$, $e_2(t_2) = \dot{e}_1(t_2) = 0$ and $\dot{e}_2(t_2) = 0$. $\sigma(t_2) = p_1 e_1(t_2) + p_2 e_2(t_2) = p_1 e(t_2)$, and (4) becomes

$$u^*(t_2) = u(t_2) + u(t_1) = \frac{JR\mu p_1}{rK_t p_2}\left[e(t_2) + e(t_1)\right]. \tag{10}$$

Substitute (10) into (2),

$$\frac{r}{J} T_d(t_2) = \mu \frac{p_1}{p_2}\left[e(t_2) + e(t_1)\right]. \tag{11}$$

If $T_d(t_1) = T_d(t_2)$, which is true in most cases, by comparing (9) with (11), $e(t_2) = 0$. This means the accuracy loss can be fully compensated.

The simplest way to inject Δu into $u(t)$ is to shift target position from y_r to $y_r' = y_r - e$, which causes the shift of origin from O to O' for $sat(\cdot)$ function, as shown in Fig. 8(b). Since d has no change, (8) becomes

$$\begin{aligned} u(t_1) &= \frac{JR\mu}{rK_t p_2}\mathrm{sat}(2p_1 e(t_1), d) \\ &= \begin{cases} 2\dfrac{JR\mu p_1}{rK_t p_2} e(t_1), & \text{if } 2p_1 e(t_1) \leq d; \\ \dfrac{JR\mu}{rK_t p_2}, & \text{if } 2p_1 e(t_1) > d. \end{cases} \end{aligned}$$

This motivates us to propose the following fine-tuning algorithm to compensate the accuracy loss by boundary layer methods.

Step1. Check the steady state error e of X/Y stage after settling down;

Step2. If $|e| > 2$ μm (10 count), adjust target position by $y_r^* = y_r - e$;

Step3. Count the loop number n for Step 1-2 and go back to Step 1;

Step4. Stop until $|e| \leq 2$ μm (10 count) or the loop number $n \geq 3$.

The flowchart of the above algorithm is shown in Fig. 10.

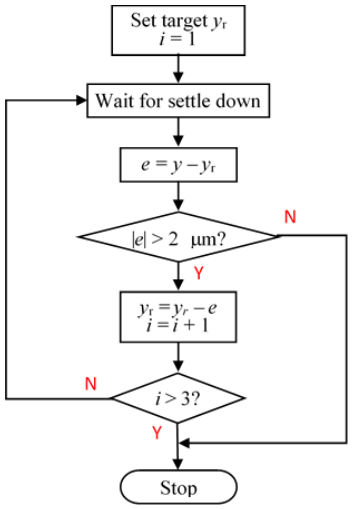

Fig. 10. Fine-tuning algorithm

IV. Validation

The validation of the proposed SMC with fine-tuning is carried on by three tests. 1) Check the effectiveness of the proposed fine-tuning. 2) Verify the accuracy and reliability of the control algorithm. 3) Compare the speed of the stage with other products. Real position is measured with SIOS Mi5000 laser interferometer and target position is read from the encoder of the stage. Error tolerance is ± 2 μm.

A. Effectiveness of the Fine-tuning

The test plan is shows as a flowchart in Fig. 11. The acceleration and max speed of the motion profile are set as 0.5 m/s^2 and 24 mm/s, respectively. SMC parameters are $p_1 = 1$, $p_2 = 0.0077$, $\mu = 1.068$ and $d = 20$ μm.

Step1. Set zero point for XY stage movement and move the stage to zero;

Step2. Towards positive direction, move XY stage with the step size of 80 μm until the stage reaches 20 mm;

Step3. Towards negative direction, move XY stage with the step size of 80 μm until the stage reaches -20 mm;

Step4. Towards positive direction, move XY stage with the step size of 80 μm until the stage reaches zero;

Step5. Repeat Step 2-4 with multiple ($2\times$, $3\times$, ..., $250\times$) step size of 80 μm.

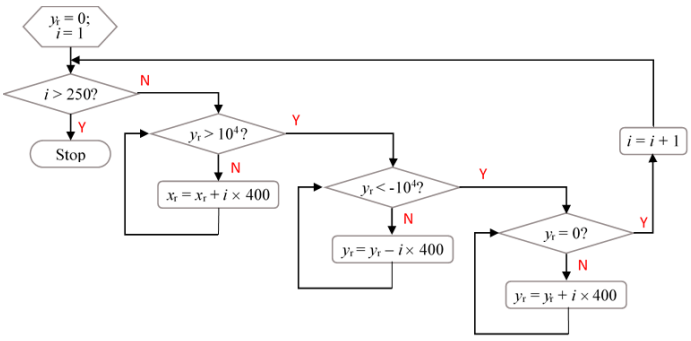

Fig. 11. Test procedures

The statistics of the test results are shown in TABLE II. For a total of 5684 target positions, standard SMC with boundary layer method achieves only 80% success rate for both X and Y stage, whereas the proposed fine-tuning algorithm increases the rate to 100%. Histogram plots in Fig. 12 show how the Gaussian distribution of position errors is squeezed to meet the precision requirements by the proposed fine-tuning algorithm.

B. Accuracy and Reliability

For the accuracy test, both transient and steady state performance are concerned.

1) Motion Profile Following: This test is to check the transient performance of the stage before it reaches the target position. X stage to move from 0 to 20 mm by following the trapezoid speed profile as shown in Fig. 7. The acceleration and max speed is the same as before. The proposed SMC with fine-tuning algorithm is compared with the original PID control in Leica DVM6. PID paprameter values are roughly identified by some trial-and-error as $K_p = 0.28$, $K_i = 0.001$ and $K_d = 0.7$, as we do not have Leica's source code. Fig. 13 shows the result, where SMC strictly follows the motion profile, but PID cannot.

2) Steady State Accuracy: 1000 target positions for X stage are randomly selected. For each one of them, steady state values of real position are recorded 500 ms later after the moving stops. The proposed SMC with fine-tuning algorithm is compared with Leica DVM6 (original PID) and Keyence VHX-6000 (stepper motor). Statistics results are shown in TABLE III. It is clear to see that the proposed method outperforms the other two with zero failure rate.

C. Stage Speed

The test for the stage speed is done by measuring the time of tile scan with different settings of zoom values, FOV and scan areas. To compare fairly, resolution of 1600×1200 pixel, exposure time of 5 ms and gain of 1.0 are in common. Three cases of different test settings are listed in TABLE IV (Case I - III) together with the scan time for PID and SMC on the same DVM6 stage. For all cases, SMC achieves at least 33% faster in stage movement than PID.

A similar tile scan test is done on Keyence VHX-6000, which uses stepper motors with open loop control. The result

TABLE II
TEST RESULTS

Total Positions	Stage	Fine-tuned?	Mean (μm)	Std (μm)	No. within ± 2 μm	% within ± 2 μm
5684	X	No	-0.0331	1.7486	4605	81.02%
		Yes	-0.0217	1.0553	5684	100%
	Y	No	0.2947	1.5438	4856	85.43%
		Yes	0.2153	1.1228	5684	100%

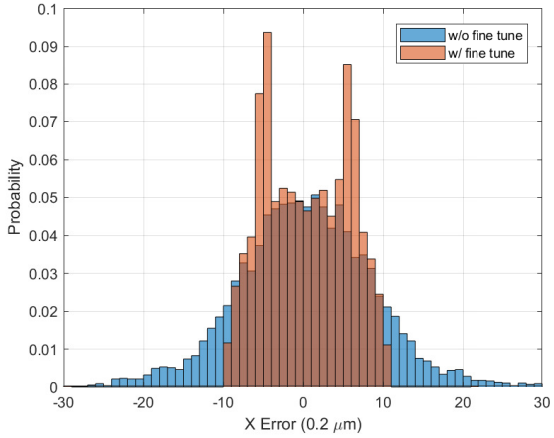

(a) Histogram for X stage

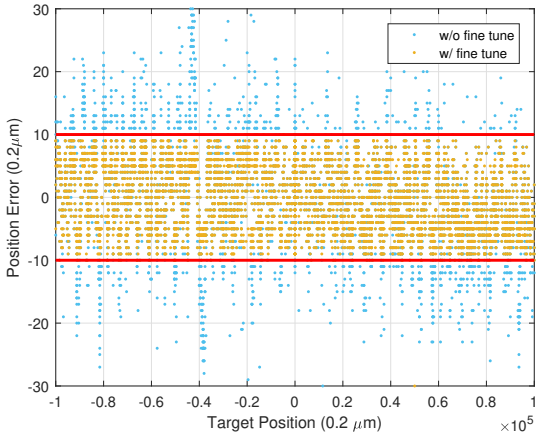

(b) Errors for X stage

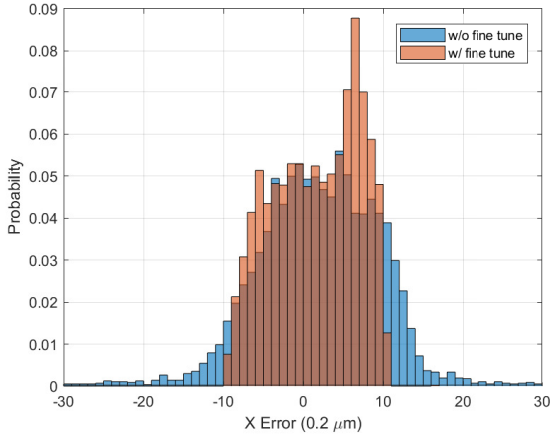

(c) Histogram for Y stage

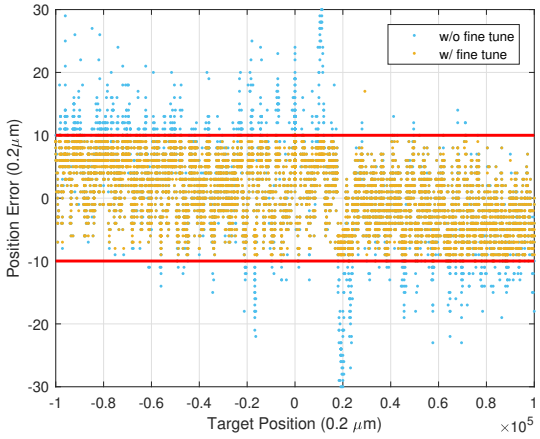

(d) Errors for Y stage

Fig. 12. Position errors before and after fine-tune

is shown in TABLE IV Case IV. Since the test is done on different microscopes, the scan time is not only dependant on the stage performance but is also affected by the speed of camera. Nevertheless, the proposed solution of DC motor with SMC still achieves comparable performance.

V. CONCLUSION

A low-cost implementation of high precision motion control for XY stage of microscope is proposed and fully analyzed in this paper. The term "low cost" refers to the fact that there is no change to the existing hardware. By changing the firmware only, ± 2 μm precision is guaranteed. The main contribution of the paper is the proposed fine-tuning algorithm for the standard SMC, which is proven to be accurate and robust in the validation test. The method can be easily extended to many other applications of motion control to improve the performance with no extra cost.

APPENDIX

For all the modeling of friction, the LuGre model is broadly accepted for its good balance between accuracy and ease of

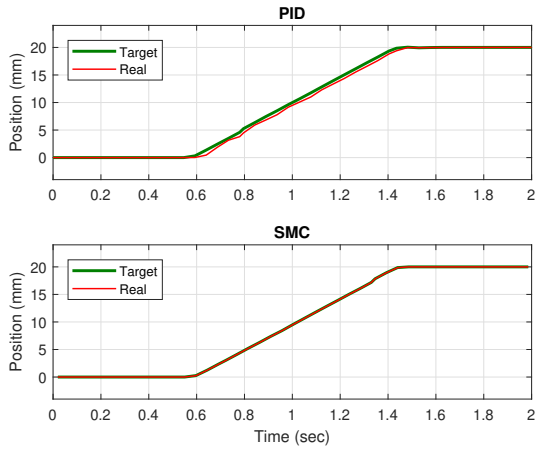

Fig. 13. Comparison between SMC and PID in motion profile following.

TABLE III
FAILURES OF 1000 RANDOM X STAGE MOVEMENTS

Stage	Target (mm)	Error (μm)	Σ	%
DVM6 (PID)	-37.904	-16	12	1.2%
	37.757	-7		
	25.659	-10		
	35.463	-15		
	29.940	-12		
	25.759	-13		
	-37.935	-11		
	33.378	-9		
	32.135	-14		
	35.403	-7		
	29.961	-7		
	35.785	-17		
VHX-6000	3.766	-5	1	0.1%
DVM6 (SMC)	-	-	0	0%

analysis. The LuGre model is described by [21]

$$\frac{dz}{dt} = v - \sigma_0 \frac{|v|}{g(v)} z, \tag{12}$$

$$F = \sigma_0 z + \sigma_1 \dot{z} + \sigma_2 v, \tag{13}$$

where v is the velocity between the two surfaces in contact, z is the internal friction state, usually interpreted as the average bristle deflection, and F is the predicted friction force. Compared with the Dahl model [22], the LuGre model has a velocity-dependent function $g(v)$ instead of a constant, a parameter σ_0 as the stiffness, an additional damping σ_1 associated with micro-displacement, and σ_2 related to the memoryless velocity-dependent viscous friction. A reasonable choice of $g(v)$ for a good approximation of the Stribeck effect is [23]

$$g(v) = F_c + (F_s - F_c)\mathrm{e}^{-|v/v_s|}, \tag{14}$$

where F_s corresponds to the stiction force, and F_c is the Coulomb friction force. v_s determines how quickly $g(v)$ approaches F_c.

REFERENCES

[1] G. Hao, "A multiaxis, large-output, sensing framework of integrating linear optical encoders for nanopositioning systems," *IEEE Sensors Letters*, vol. 1, DOI 10.1109/LSENS.2017.2697074, no. 3, pp. 1–4, Jun. 2017.

[2] J. Yu, Y. Xie, Z. Li, and G. Hao, "Design and experimental testing of an improved large-range decoupled xy compliant parallel micromanipulator," *Journal of Mechanisms Robotics*, vol. 7, DOI 10.1115/1.4030467, no. 4, 2015.

[3] Z. Zhang, P. Yan, and G. Hao, "A large range flexure-based servo system supporting precision additive manufacturing," *Engineering*, vol. 3, DOI 10.1016/J.ENG.2017.05.020, no. 5, p. 708, 2017. [Online]. Available: http://engineering.org.cn/EN/abstract/article_12442.shtml

[4] D. R. McMurtry and I. S. Bennell, "Sample positioning stage and method of operation," U.S. Patent 8 254 002 B2, Jul. 17, 2008.

[5] H. Olsson, K. J. Åström, C. C. de Wit, M. Gäfvert, and P. Lischinsky, "Friction models and friction compensation," *European Journal of Control*, vol. 4, no. 3, pp. 176 – 195, 1998.

[6] V. I. Utkin, *Sliding modes in control and optimization*. Berlin: Springer-Verlag, 1992.

[7] V. Utkin and H. Lee, "Chattering problem in sliding mode control systems," in *International Workshop on Variable Structure Systems, 2006. VSS'06.*, pp. 346–350, Jun. 2006.

[8] J. A. BURTON and A. S. I. ZINOBER, "Continuous approximation of variable structure control," *International Journal of Systems Science*, vol. 17, no. 6, pp. 875–885, 1986.

[9] A. Sabanovic, "Variable structure systems with sliding modes in motion control—A survey," *IEEE Transactions on Industrial Informatics*, vol. 7, no. 2, pp. 212–223, May. 2011.

[10] A. Rosales, Y. Shtessel, L. Fridman, and C. B. Panathula, "Chattering analysis of HOSM controlled systems: Frequency domain approach," *IEEE Transactions on Automatic Control*, vol. 62, no. 8, pp. 4109–4115, Aug. 2017.

[11] L. Wu, S. K. Mazumder, and O. Kaynak, "Sliding mode control and observation for complex industrial systems—Part I," *IEEE Transactions on Industrial Electronics*, vol. 64, no. 8, pp. 6680–6683, Aug. 2017.

[12] M.-L. Tseng and M.-S. Chen, "Chattering reduction of sliding mode control by low-pass filtering the control signal," *Asian Journal of Control*, vol. 12, no. 3, pp. 392–398, 2010.

[13] J. X. Xu and K. Abidi, "Discrete-time output integral sliding-mode control for a piezomotor-driven linear motion stage," *IEEE Transactions on Industrial Electronics*, vol. 55, no. 11, pp. 3917–3926, Nov. 2008.

[14] K. Abidi, J. X. Xu, and Y. Xinghuo, "On the discrete-time integral sliding-mode control," *IEEE Transactions on Automatic Control*, vol. 52, no. 4, pp. 709–715, Apr. 2007.

[15] G. Bartolini, A. Ferrara, E. Usai, and V. I. Utkin, "On multi-input chattering-free second-order sliding mode control," *IEEE Transactions on Automatic Control*, vol. 45, no. 9, pp. 1711–1717, Sep. 2000.

[16] S. Ding, J. Wang, and W. X. Zheng, "Second-order sliding mode control for nonlinear uncertain systems bounded by positive functions," *IEEE Transactions on Industrial Electronics*, vol. 62, no. 9, pp. 5899–5909, Sep. 2015.

[17] V. Utkin, "Discussion aspects of high-order sliding mode control," *IEEE Transactions on Automatic Control*, vol. 61, no. 3, pp. 829–833, Mar. 2016.

[18] V. I. Utkin and A. S. Poznyak, "Adaptive sliding mode control with application to super-twist algorithm: Equivalent control method," *Automatica*, vol. 49, no. 1, pp. 39 – 47, 2013.

[19] I. L. H. Lim and D. Yang, "Low-cost precision motion control for industrial digital microscopy," in *IECON 2017 - 43rd Annual Conference of the IEEE Industrial Electronics Society*, pp. 7281–7287, Oct. 2017.

[20] V. Stimpson, B. Smith, A. Woolfrey, and M. Hill, "Sample positioning apparatus," U.S. Patent 0 310 215 A1, Jun. 30, 2009.

[21] K. J. Åström and C. C. de Wit, "Revisiting the LuGre friction model," *IEEE Control Systems Magazine*, vol. 28, no. 6, pp. 101–114, 2008.

[22] P. Dahl, "A solid friction model," The Aerospace Corporation, El Segundo, CA, Technical Report TOR-0158(3107-18)-1, 1968.

[23] A. Tustin, "The effects of backlash and of speed-dependent friction on the stability of closed-cycle control systems," *Journal of the Institution of Electrical Engineers Part 1 General*, vol. 94, pp. 143–151, 1947.

TABLE IV
SPEED TEST RESULTS FROM TILE SCAN

Case	Zoom	FOV X×Y	Scan Area	Time Consumption	
				Counterpart	Proposed
I	10×	1 (mm)×0.75 (mm)	10 (mm)×7.5 (mm)	98 (s)	51 (s)
II	5×	2 (mm)×1.5 (mm)	20 (mm)×15 (mm)	96 (s)	58 (s)
III	2×	5 (mm)×3.75 (mm)	50 (mm)×37.5 (mm)	100 (s)	67 (s)
IV	2.93×	3.4 (mm)×2.5 (mm)	14 (mm)×15 (mm)	31 (s)	37 (s)

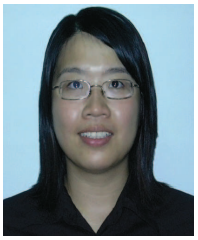

Li Hong Idris Lim (M'14) received the B.Eng. and Ph.D. degrees in electrical engineering from the National University of Singapore, Singapore.

From 2008 to 2012, she was with Vestas Technology R&D. Since 2013, she has been a full-time Assistant Professor with the University of Glasgow, Glasgow, U.K. Her research interests include control of wind energy systems, solar forecasting and system identification, and smart grids.

Dazhi Yang received the B.Eng., M.Sc., and Ph.D. degrees in electrical engineering from the National University of Singapore, Singapore, in 2009, 2012, and 2015, respectively.

Currently, he is a Research Fellow with Singapore Institute of Manufacturing Technology (SIMTech), Agency for Science, Technology and Research (A*STAR), Singapore. His research interests include forecasting and spatio-temporal statistics.